Flux-line lattice in uniaxial superconductors at low magnetic inductions

L. L. Daemen and L. J. Campbell*
Theoretical Division, Los Alamos National Laboratory, Los Alamos, New Mexico 87545

V. G. Kogan
Ames Laboratory and Department of Physics, Iowa State University, Ames, Iowa 50011
(Received 2 March 1992)

Within the London approximation, we predict the geometry of the flux lattice in anisotropic, strongly type-II superconductors for arbitrary field orientation and intensity. At low magnetic fields, the scaling of the lattice parameters with field differs markedly from the ordinary $B^{-1/2}$ dependence. We also calculate the form factors and reflectivities for neutron diffraction. The dependence of the reflectivity on the angle between the magnetic field and the c axis, and on the field intensity, is calculated.

I. INTRODUCTION

One of the most interesting aspects of high-temperature superconductivity is the exact nature of the intermediate state, characterized by the penetration of the magnetic flux into the sample in the form of quantized flux lines. In particular, the detailed structure of such a flux line in the highly anisotropic and inhomogeneous high-temperature superconductors, as well as their arrangement in a regular lattice, has been lately the object of much discussion.[1] The phenomenon of vortex attraction in anisotropic superconductors[2,3] when the field is not parallel to one of the principal axes of the crystal has very interesting consequences, some of which are examined below. At large magnetic fields, the flux lattice structure was predicted by Campbell, Doria, and Kogan.[4] Their calculation is, however, not valid in the low-field limit. Since the low-field limit is important for a number of experimental techniques such as decoration experiments or muon spin rotation, it is interesting to investigate how the lattice geometry scales with magnetic field near the lower critical field. From a theoretical point of view, the calculation of quantities such as the elastic constants of the flux-line lattice requires the exact flux lattice geometry. The use of lattice geometries that do not correspond to an equilibrium configuration leads to unphysical results such as negative elastic constants.

A number of decoration experiments performed during the past three years have shed some light on the issue of the geometrical arrangement of the flux lines.[5] The decoration method probes vortex positions at the surface and is limited to low fields by its inherent resolution. Other techniques, such as muon spin rotation as (μSR), are sensitive to the bulk magnetic-field distribution, but provide only indirect information on the structure of the flux-line lattice (FLL). A more direct way to study the characteristics of the FLL is the diffraction of subthermal neutrons. It has proved to be a useful technique to probe directly the FLL at the microscopic level. Since the measurements of Cribier *et al.*[6] this technique has been developed extensively and applied to a large class of superconducting materials.[7] However, it is only recently that the technique was applied to high-T_c superconductors by Forgan *et al.*[8] We discuss their results briefly.

II. THE EQUILIBRIUM FLL

The basic equation describing the magnetic-field distribution of an isolated flux line has been known for a long time.[9] Within the London approximation, it reads

$$b_s+\lambda^2 m_{ij}\epsilon_{jpq}\epsilon_{irs}\partial_r\partial_p b_s=\Phi_0\delta_{sz}\delta(\mathbf{r}) , \tag{1}$$

where m_{ij} is the mass tensor. In the crystal frame, and for a uniaxial material, m is diagonal: $m=\mathrm{diag}(m_a,m_a,m_c)$ and is normalized so that $\det m=1$. $r,p=x,y$ and $s,q,i,j=x,y,z$. The anisotropy ratio is defined by

$$\gamma=(m_c/m_a)^{1/2}=\frac{\lambda_c}{\lambda_{ab}} . \tag{2}$$

It should be emphasized that the London limit was chosen deliberately for several reasons. First of all, most high-temperature superconductors are high-κ materials, a condition required to be in the domain of validity of the London approximation. Second, the London equation is a linear partial differential equation. It can be solved analytically in Fourier space. The anisotropy of the superconductor is taken into account via the introduction of a mass tensor. The material is still assumed to be homogeneous. One can question this assumption considering the layered nature of most of the high-T_c materials. However, there are good indications that the London model can predict reliably a number of magnetic properties (except when the external field is close to the ab planes, in which case the inhomogeneity of the material has to be accounted for explicitly[10]).

The solution to Eq. (1) in Fourier space is given by

$$b_x(\mathbf{q})=\frac{\Phi_0\lambda^2 m_{zx}q_y^2}{D(\mathbf{q})} , \tag{3}$$

$$b_y(\mathbf{q})=-\frac{\Phi_0\lambda^2 m_{zx}q_x q_y}{D(\mathbf{q})}=-\frac{q_x}{q_y}b_x(\mathbf{q}) , \tag{4}$$

$$b_z(\mathbf{q})=\frac{\Phi_0(1+\lambda^2 q^2 m_{zz})}{D(\mathbf{q})} , \tag{5}$$

$$D(\mathbf{q})=(1+\lambda^2 q^2 m_{zz})(1+\lambda^2 q_y^2 m_{xx}+\lambda^2 q_x^2 m_{yy}) -\lambda^4 q^2 m_{xz}^2 q_y^2 , \tag{6}$$

where $q^2=q_x^2+q_y^2$. The various components of the mass tensor in the vortex frame are given by

$$m_{xx}=m_a\cos^2\theta+m_c\sin^2\theta,\quad m_{xy}=0=m_{yz} ,$$
$$m_{yy}=m_a ,\quad m_{zz}=m_a\sin^2\theta+m_c\cos^2\theta , \tag{7}$$
$$m_{xz}=(m_a-m_c)\sin\theta\cos\theta ,$$

θ is the angle between the vortex axes and the c axis. We can invert this Fourier transform numerically to look at the magnetic-field distribution in real space. Since b_z is (up to a numerical factor) the interaction potential (per unit length) between two parallel infinite flux lines, it is worth describing $b_z(x,y)$ in some detail. A plot of the transverse field components b_x and b_y can be found in Ref. 3. Figure 1 shows $b_z(x,y)$ in the plane perpendicular to the flux-line axis. A number of remarkable features are immediately noticeable. First of all, the field changes sign in two regions of the xy plane, i.e., the vortex-vortex potential is attractive in part of those regions. Notice the presence of two minima in the field distribution on each side of the vortex core in the regions where the potential is negative. The potential is repulsive in the direction perpendicular to the line joining the minima. The formation of vortex "chains," to be described in more detail below, can be directly related to this peculiar form of the vortex-vortex interaction potential.

The total (London) energy (per unit length) of a system of flux lines is

$$E=\sum_{i<j} b_z(\mathbf{r}_i-\mathbf{r}_j)+\sum_i \sigma_i , \tag{8}$$

where σ_i is the self-energy (per unit length) of the ith vortex. An explicit expression for σ_i can be found in Ref. 11. In Eq. (8), E appears as a function of the vortex positions $\{\mathbf{r}_i\}$. Ideally, one should minimize E with respect to the positions and find the configuration that leads to the absolute energy minimum. We performed such numerical minimizations.[12] These computer simulations are time consuming and ineffective if we want to study systematically the flux lattice geometry for arbitrary field orientation and intensity. We can simplify the problem considerably by noting that the equilibrium configuration is a regular periodic lattice, and by assuming that the unit cell has the geometry shown in Fig. 2 and contains one flux quantum per unit cell. Notice that in Fig. 2, the triangle AOB is isosceles. The validity of the latter assumption was confirmed by numerous computer minimizations of the total energy, Eq. (8). Thus we can minimize the energy per unit cell rather than the total energy of the lattice, and express the energy (per unit cell) in terms of one variable only, namely $\rho\equiv a/b$, the ratio of the flux lattice parameters. Rather than using the energy expressed in terms of the real-space fields

$$e[\mathbf{B}(\mathbf{r})]=\int\int_{\text{u.c.}} d^2r\frac{1}{2\mu_0}\{|\mathbf{B}(\mathbf{r})|^2+\lambda^2[\nabla\times\mathbf{B}(\mathbf{r})]_i \times m_{ij}[\nabla\times\mathbf{B}(\mathbf{r})]_j\} , \tag{9}$$

where $\mathbf{B}$ is the total magnetic field at $\mathbf{r}$:

$$\mathbf{B}(\mathbf{r})=\sum_{\mathbf{R}_{mn}} \mathbf{b}(\mathbf{r}-\mathbf{R}_{mn}) , \tag{10}$$

it is easier to start with the total energy expressed in terms of the Fourier components of $\mathbf{b}$

$$e=\frac{1}{2\mu_0}\frac{1}{F_c}\sum_{\mathbf{G}}\{|\mathbf{b}(\mathbf{G})|^2+\lambda^2[\mathbf{G}\times\mathbf{b}(\mathbf{G})]_i m_{ij}[\mathbf{G}\times\mathbf{b}(\mathbf{G})]_j\} , \tag{11}$$

where F_c is the unit-cell area. The lattice vectors are given by

$$\mathbf{R}_{mn}=(ma+nb\cos\psi)\hat{\mathbf{x}}+nb\sin\psi\hat{\mathbf{y}} , \tag{12}$$

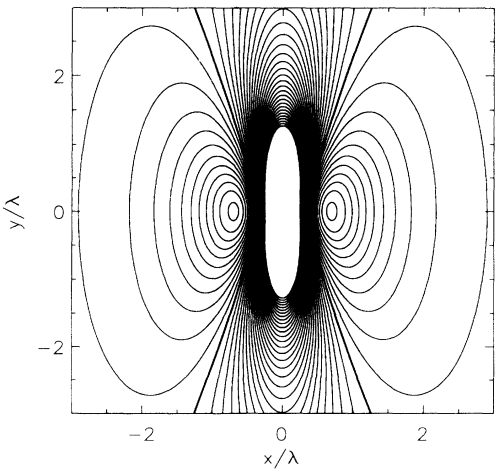

FIG. 1. Distribution of the z component of the magnetic field setup by anisolated flux line in a plane perpendicular to the flux line. The field vanishes along the thick solid lines. It is positive in the central region near the core and negative in the two regions to the left and right of the central area. The contours are equidistant ($\gamma=55$, $\theta=60°$, $\kappa=60$).

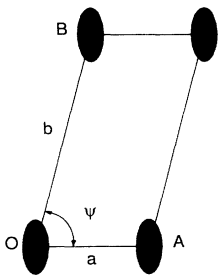

FIG. 2. Unit-cell geometry assumed for the energy minimization. OAB is an isosceles triangle.

where m,n are integers. The summation in Eq. (11) is over the reciprocal lattice vectors:

$$\mathbf{G}_{mn}=n\frac{2\pi}{a}\hat{x}+\left[m\frac{2\pi}{b}-n\frac{2\pi}{a}\cos\psi\right]\frac{1}{\sin\psi}\hat{y}\ . \tag{13}$$

In Eqs. (12) and (13), a, b, and ψ depend on ρ (and the magnetic induction B) in the following way:

$$a=\left[\frac{\Phi_0}{B}\frac{\rho}{[1-(\rho/2)^2]^{1/2}}\right]^{1/2}, \tag{14}$$

$$b=\left[\frac{\Phi_0}{B}\frac{1}{\rho[1-(\rho/2)^2]^{1/2}}\right]^{1/2}, \tag{15}$$

$$\cos\psi=\frac{\rho}{2}\ . \tag{16}$$

In deriving Eqs. (14)–(16), we have used the geometry defined in Fig. 2. The reciprocal lattice vectors depend on ρ via a, b, and ψ, and the total energy depends on ρ via the reciprocal lattice vectors.

Care must be taken in the calculation of the total energy per unit cell e. Formally, the expression, Eq. (11), is divergent because in the London approximation the magnetic field has a singularity at $\mathbf{r}=\mathbf{0}$. This singularity must be removed by truncating the field at (roughly) ξ, the coherence length. ξ is the length scale below which the London description ceases to be valid and determines the vortex core dimensions. Since the core is elliptic in an anisotropic material, as can be inferred from Fig. 1, we use an elliptic cutoff as suggested by Brandt.[16] The coherence lengths in the ab plane and along the c axis are ξ_{ab} and ξ_c, respectively. These lengths are such that $\gamma=\xi_{ab}/\xi_c$. One can define an average coherence length $\xi=(\xi_{ab}^2\xi_c)^{1/3}$. We took $\kappa=\lambda/\xi=60$, a value suggested by recent μSR measurements on $YBa_2Cu_3O_{7-x}$ (YBCO) single crystals.[13] This cutoff prescription is approximate, but acceptable at low magnetic inductions. We tested different cutoff prescriptions and checked that the results were insensitive to the method used to remove the divergence. At larger magnetic inductions, a resolution of the full Ginzburg-Landau equations would be required. The minimization of Eq. (11) with respect to ρ can be performed in a number of ways. We chose the golden-section-search method[14] because of its robustness and also because the derivatives of e with respect to ρ are not readily available. The minimum in the London energy considered as a function of ρ is very shallow, especially at low inductions and small angles. This makes the minimization procedure rather difficult, and requires high accuracy in the calculation of the energy. Alternative schemes exist to facilitate the calculation of the lattice energy.[15]

The results of applying this minimization procedure are shown in Figs. 3(a) and 3(b) for $\gamma=5$ and 55, respectively. Those are the values usually quoted for $YBa_2Cu_3O_7$ and $Bi_2Sr_2CaCu_2O_8$ (BSCCO). When $\theta=0$, $\rho=1$ and the lattice is a regular triangular lattice, as expected. However, as θ increases, ρ decrease very rapidly, especially when γ is large. This leads to a lattice configuration where the lattice parameter a is much smaller than b, i.e., the lattice appears as a highly distorted triangular lattice. In the extreme situation where $\rho\ll 1$, the lattice appears as a series of parallel "chains" of vortices. Physically, this behavior is easy to understand: As pointed out above, the interaction potential between two flux lines has a pronounced (attractive) minimum on each side of the vortex core. The presence of these minima strongly favors the alignment of the flux lines and the formation of chains. There is more to be said about the field dependence of the lattice geometry. The applied magnetic field determines the surface flux-line density: $n=B/\Phi_0$ where Φ_0 is the flux quantum and B the magnetic induction. In an isotropic superconductor, the lattice is triangular with one flux quantum per unit cell. The lattice parameters are given by $a=b=(2\Phi_0/B/\sqrt{3})^{1/2}$, i.e., the lattice scales uniformly in all directions with $B(a,b\simeq B^{-1/2})$. Figures 4(a) and 4(b) show the lattice parameters vs field for various field orientations. The plots are log-log plots so that the slope of the various curves are a direct measure of the field scaling exponents. It is obvious that at low magnetic field the lattice constants do not scale uniformly with field. The separation of two flux lines in a chain a remains con-

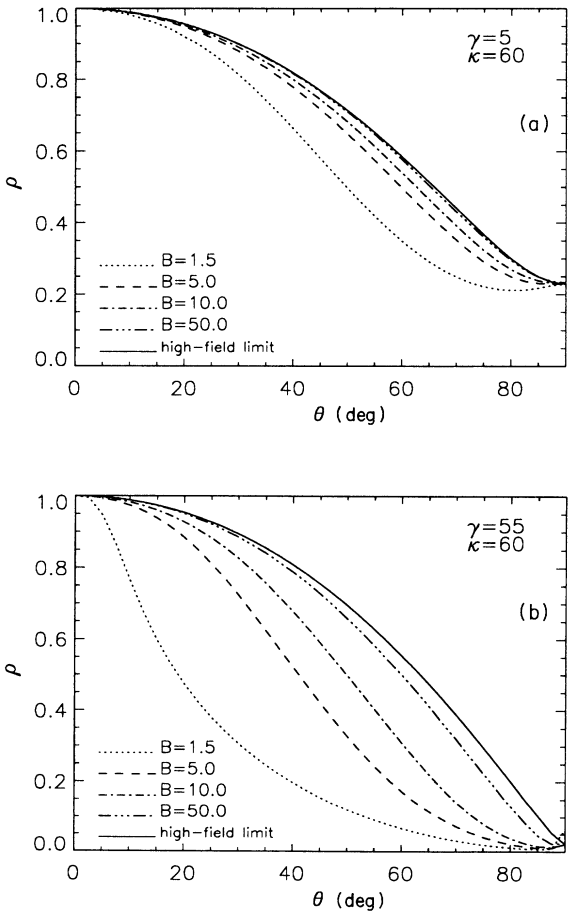

FIG. 3. (a) Ratio for the flux lattice parameters: $\rho=a/b$ vs θ, the angle between the vortices and the c axis for various magnetic fields. $\gamma=5$; (b) $\gamma=55$. The magnetic field is in units of $\Phi_0/(2\pi\lambda^2)$ where $\lambda=(\lambda_{ab}^2\lambda_c)^{1/3}$.

stant and independent of field at low fields (and over a rather large range of magnetic field when $\gamma=55$). Since there must be exactly one flux quantum per unit cell, the other lattice constant b must scale as $b\simeq B^{-1}$. Therefore, at low fields, the chain structure is fixed (determined by the position of the minimum in the vortex-vortex interaction potential) and it is the separation between two chains that shows all the magnetic-field dependence. The interaction between two adjacent chains is very weak. At larger magnetic fields, as the chains begin to interact more strongly, this peculiar behavior disappears and the scaling reverts to an ordinary $B^{-1/2}$ scaling for the lattice constants a and b. Notice that this "scaling crossover" happens abruptly at some critical field. Above this crossover field, the lattice is just a distorted triangular lattice scaling uniformly in all directions with increasing magnetic field. Strictly speaking, the use for the term "vortex chains" should be applied to describe the situation $a\simeq$const and $b\simeq B^{-1}$. For $\theta=\pi/2$, the vortex-vortex potential is again purely repulsive, and the magnetic field scaling is the ordinary $B^{-1/2}$ dependence. Finally, it is worth pointing out that at large magnetic fields the ρ vs θ curves collapse on the same "universal" curve [the solid line in Figs. 3(a) and (b)] regardless of field intensity. This curve is the curve obtained by Campbell, Doria, and Kogan.[4]

It should be emphasized that the results presented in this section describe how the flux lattice scales with the average magnetic induction **B**. Similarly, the angle θ gives the orientation of the magnetic induction, as opposed to the orientation of the applied magnetic field, $\mathbf{H}_{app}$. At low fields, the orientations of **B** and $\mathbf{H}_{app}$ are likely to differ significantly. Grishin, Matynovich, and Yampol'skii have calculated, in the very-low-field limit, the relative orientation of **B** and $\mathbf{H}_{app}$ as a function of the external field intensity and orientation.[3] We did not include any demagnetization effect due to finite-size effects: Our results are valid for an infinite superconducting medium only.

III. INTEGRATED REFLECTIVITY

The general formalism to calculate the integrated reflectivity R_{hk} is well established,[7] and we shall merely quote the relevant results. In the Born approximation, the differential cross section for the elastic scattering of a

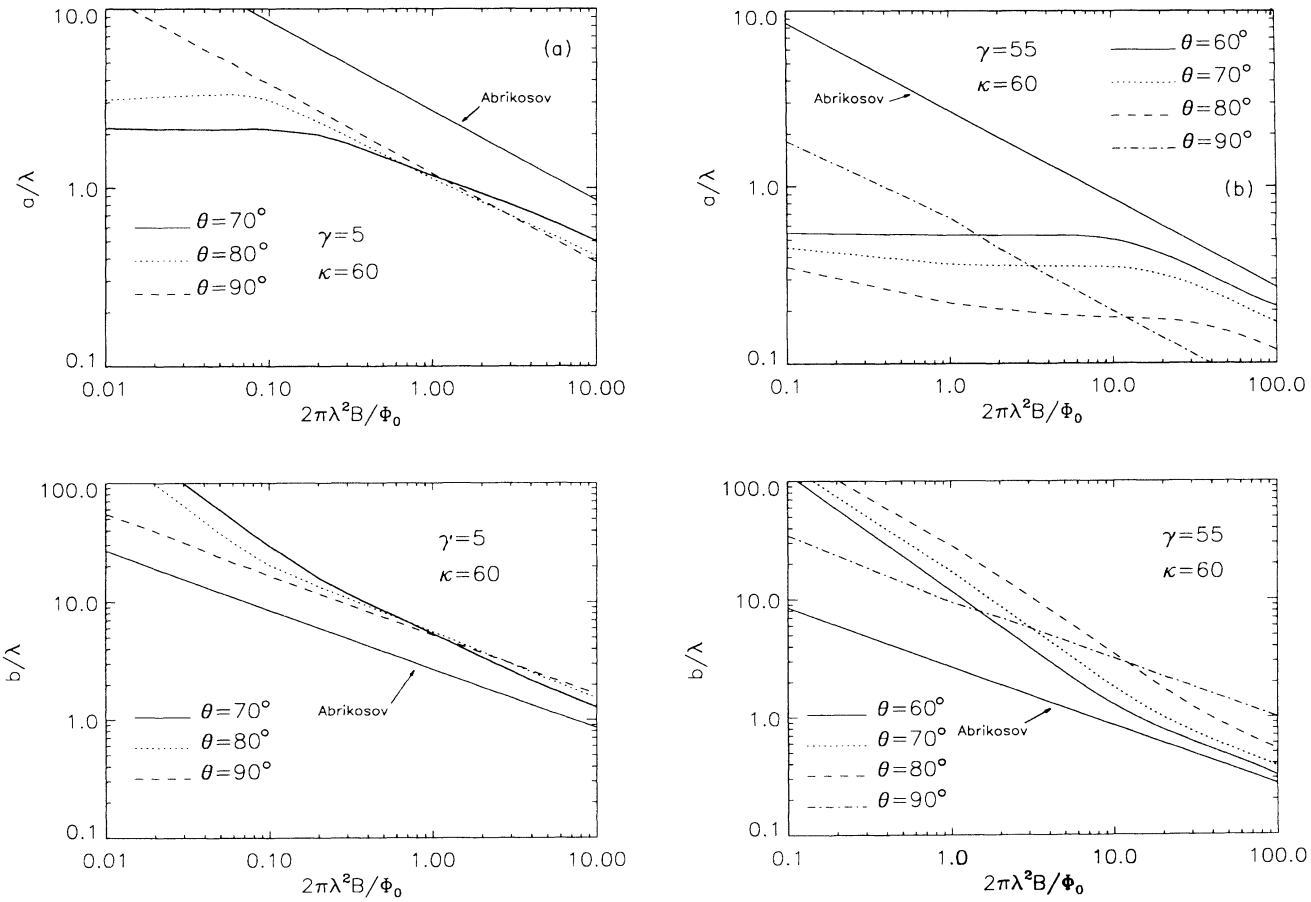

FIG. 4. (a) Flux lattice parameters a and b is magnetic induction for various value of θ, the angle between the vortices and the c axis. $\gamma=5$; (b) $\gamma=55$. The magnetic field is in units of $\Phi_0/(2\pi\lambda^2)$ where $\lambda=(\lambda_{ab}^2\lambda_c)^{1/3}$. The chainlike dependence of the flux lattice parameters at low fields reverts to the usual $B^{-1/2}$ dependence as θ approaches $\pi/2$ as it should.

neutron beam by an array of scatterers is

$$\frac{d\sigma}{d\Omega}=\left[\frac{M_n}{2\pi\hbar^2}\right]^2\sum_{\sigma}\sum_{\sigma'}p_\sigma|\langle\mathbf{k}'\sigma'|V|\mathbf{k}\sigma\rangle|^2$$
$$=\sum_{\sigma}p_\sigma\langle\sigma|W^\dagger W|\sigma\rangle\ , \tag{17}$$

where

$$W=\langle\mathbf{k}'|V|\mathbf{k}\rangle \tag{18}$$

is an operator acting on spin states. V is the interaction between a neutron and the flux lines. p_σ describes the beam polarization, M_n is the neutron mass, and $|\mathbf{k}\sigma\rangle$ is a neutron quantum state. For an unpolarized beam, $p_\sigma=\frac{1}{2}$ and

$$\frac{d\sigma}{d\Omega}=\frac{1}{2}\left[\frac{M_n}{2\pi\hbar^2}\right]^2[\langle+|W^+W|+\rangle+\langle-|W^+W|-\rangle]\ . \tag{19}$$

The interaction between the neutron spin $\mathbf{S}$ and the magnetic induction $\mathbf{B}$ set up by the array of flux lines is

$$V(\mathbf{r})=-\gamma(\mu_B/\hbar)\mathbf{S}\cdot\mathbf{B}(\mathbf{r})$$
$$=-(\gamma/2)\mu_B(B_xS_x\sigma_x+B_yS_y\sigma_y+B_zS_z\sigma_z)\ , \tag{20}$$

where σ_x, σ_y, and σ_z are the Pauli matrices, $\mathbf{S}=(S_x,S_y,S_z)$ is a unit vector indicating the spin direction, and γ the neutron gyromagnetic ratio. Notice that $\mathbf{B}(\mathbf{r})$ is the total magnetic induction at $\mathbf{r}$. The final result is easily expressed in terms of the Fourier components of the magnetic induction set up by *one* flux line:

$$\frac{d\sigma}{d\Omega}=\left[\frac{\gamma\mu_B}{2}\right]^2\left[\frac{M_n}{2\pi\hbar^2}\right]^2\sum_{\mathbf{G}}[|b_x(\mathbf{G})|^2+|b_y(\mathbf{G})|^2$$
$$+|b_z(\mathbf{G})|^2]\delta(\mathbf{q}-\mathbf{G})\ , \tag{21}$$

where $\mathbf{G}$ is a reciprocal lattice vector of the flux-line lattice, $\mathbf{q}$ is the momentum transfer, and the $b_i(\mathbf{G})$'s, $(i=x,y,z)$ are given by Eqs. (3)–(6). The experimentally measured quantity is the integrated reflectivity. It is obtained directly from the scattering cross section upon integration over the solid angle Ω. For the (hk) Bragg peak, the integrated reflectivity is

$$R_{hk}=2\pi\left[\frac{\gamma_n}{4}\right]^2\frac{\lambda_n^2}{G_{hk}}\frac{V}{F_c^2}|F_{hk}|^2\ , \tag{22}$$

where γ_n is the ratio of the neutron magnetic moment to the nuclear magneton ($\gamma_n=1.91$), λ_n is the neutron wavelength, V is the irradiated sample volume, G_{hk} is the magnitude of the reciprocal lattice vector corresponding to the (hk) Bragg peak, and F_c is the FLL unit-cell area. The form factor for the (hk) reflection is determined below. Physically, R_{hk} is the ratio of the total intensity of the (hk) reflection to the unscattered neutron flux behind the sample. It has dimension of an area, and gives the total scattering cross section. We now proceed to a systematic discussion of the various factors appearing in Eq. (22).

The cell area is $F_c=\Phi_0/B$. The reciprocal lattice vector corresponding to the (hk) reflection is given by Eq. (13). Finally, the form factor F_{hk} is the normalized Fourier transform of the two-dimensional magnetic-field distribution of a *single* flux line:

$$F_{hk}=\frac{\int d^2r\,b(\mathbf{r})\exp(i\tau_{hk}\cdot\mathbf{r})}{\int d^2r\,b(\mathbf{r})}=\frac{|\mathbf{b}(\mathbf{G})|^2}{\Phi_0}\ . \tag{23}$$

Everything else being constant, the form factor for a given reflection is inversely proportional to λ^2. Since the form factor appears squared in Eq. (22) for the reflectivity, we expect the large London penetration depth in the oxide superconductors to suppress the reflected intensity considerably compared to what one would expect in a conventional superconductor with smaller λ. Equivalently, we can say that because of the large penetration depth, the magnetic field of a single flux line penetrates far inside the sample. The superposition of these individual contributions will produce a very uniform microscopic field. Since neutron diffraction is sensitive to variations in the magnetic field, the resulting scattering intensity will be low. Other imperfections in the materials' microstructure will contribute to a decrease in the intensity of the scattering. For example, in a polycrystalline material the presence of grain boundaries will cause the flux lines to bend irregularly to take advantage of the intergrain space to lower their self-energy. This bending will further disrupt locally the periodicity of the magnetic field.

We focused on the (10) peak because it is presumably the most intense, and also because, as discussed in Sec. II, the spacing between the flux lines is more regular along the chains than in the direction orthogonal to the chains. This is because the spacing between two vortices in a chain is determined, at low field, by the position of the minima in the vortex-vortex potential. Figures 5(a) and 5(b) show the integrated reflectivity as a function of magnetic induction for $\gamma=5$ and $\gamma=55$, respectively. The reflectivity is very low for $\gamma=5$ or $\gamma=55$, and decreases rapidly as the magnetic induction is tilted away from the c axis. For $\theta=90°$, the reflectivity is suppressed by two orders of magnitude compared to the $\theta=0°$ reflectivity. It is interesting to point out that the reflectivity for $\gamma=55$ is not as low as one might have expected. This is because the larger anisotropy of the material yields a more anisotropic vortex-vortex potential, which in turn leads to a more inhomogeneous microscopic field distribution, and a larger form factor. At large magnetic inductions, the reflectivity decreases slowly as $B^{1/2}$, as can be inferred easily from the magnetic induction dependence of the various factors appearing in Eq. (22).

Recent neutron-diffraction measurements by Forgan *et al.*[8] show very clearly a highly symmetric diffraction pattern in YBCO single crystals when the field is applied parallel to the c axis. The diffraction pattern has a fourfold symmetry instead of the expected sixfold symmetry. The fact that the Bragg spots coincide with the direction of the twinning planes ([110] and [1$\bar{1}$0]) in the crystal

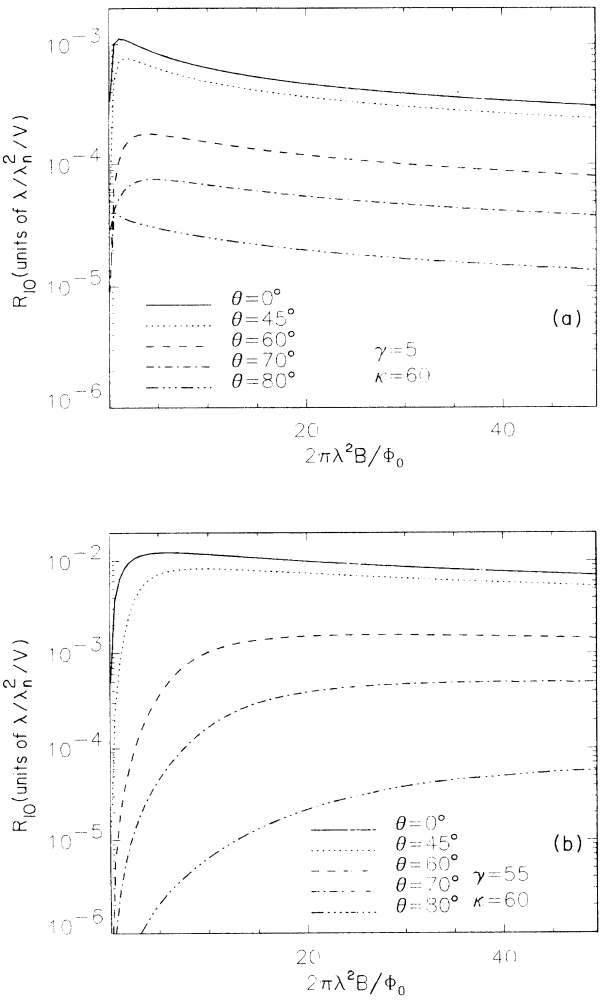

FIG. 5. (a) Neutron-diffraction integrated reflectivity for the (10) Bragg reflection for (a) $\gamma=5$ and (b) $\gamma=55$. λ is the average penetration depth, V is the volume of the sample, and λ_n is the neutron wavelength.

clearly indicates that the flux lines are heavily pinned by the twin boundaries which thus dictate the symmetry of the flux lattice. Forgan *et al.* also tilted the magnetic field so that the angle between the external magnetic field and the c axis was equal to 45°. They observed a distorted sixfold symmetric diffraction pattern with two of the diffraction spots being clearly more intense than the other four. Again, the most intense diffraction peaks occurred in the direction for the twinning planes. Of course, since the field is tilted with respect to the c axis, only one set of twin planes is likely to play a significant role in pinning the flux lines along their length, and this only if the applied magnetic field is parallel to the twin planes. Pinning by twin planes has been confirmed very clearly by Vinnikov *et al.* in their decoration experiments.[17] Although the observation of Bragg peaks by Forgan *et al.* is very encouraging, it is unlikely that it will help confirm our predictions, unless similar measurements are repeated on untwinned YBCO crystal or on Bi or Tl compounds, which have no twin boundaries. The theoretical results presented above show that the reflectivity is not significantly smaller in more anisotropic crystals.

IV. CONCLUSIONS

We showed that in anisotropic superconductors, the low-field flux lattice geometry is nontrivial, and scales with field in a peculiar way. In superconductors with a fairly low anisotropy, this unusual scaling behavior may not be directly observable because it takes place below the lower critical magnetic field. For instance, if $\lambda_{ab}=150$ nm, and $\gamma=5$, then $\Phi_0/(4\pi\lambda^2)\ln\kappa\simeq 5$ mT, which is probably below the lower critical field for all vortex orientations. However, for $\gamma=55$, the behavior should be observable at fields equal to several times the lower critical field. The recent observation of vortex chains by Bolle *et al.*[5] in decoration experiments on BSCCO samples seems to confirm the existence of chains. What they observed is, however, more complex than the simple flux lattice described here. The exact reason for this is not known. It could be that surface effects (possibly important in the thin slabs used in the experiment) and/or pinning effects prevent the formation of the ideal lattice discussed above. More neutron or μSR studies in larger samples, and at larger fields should help clarify the situation.

Similar calculations for the more complicated case of a biaxial superconductor are in progress. The results will be published elsewhere.

ACKNOWLEDGMENTS

We gratefully acknowledge useful conversations with T. O. Brun, E. M. Forgan, and T. M. Riseman. This work was supported by the U.S. Department of Energy.

*Present address: National High-Magnetic Field Laboratory, MS-K765, Los Alamos National Laboratory, Los Alamos, NM 87545.

[1]For a recent review, see E. H. Brandt, Int. J. Mod. Phys. B **5**, 751 (1991).

[2]A. I. Buzdin and A. Yu. Simonov, Pis'ma Zh. Eksp. Teor. Fiz. **51**, 168 (1990) [JETP Lett. **51**, 191 (1990)]; Physica B **165/166**, 101 (1990); A. V. Balatskii, L. I. Burlachkov, and L. P. Gor'kov, Zh. Eksp. Toer. Fiz. **90**, 1478 (1986) [Sov. Phys. JETP **63**, 866 (1986)].

[3]A. M. Grishin, A. Yu. Matynovich, and S. V. Yampol'skii, Zh. Eskp. Teor. Fiz. **97**, 1930 (1990); Physica B **165/166**, 1103 (1990).

[4]L. J. Campbell, M. M. Doria, and V. G. Kogan, Phys. Rev. B **38**, 2439 (1988).

[5]P. L. Gammel *et al.*, Phys. Rev. Lett. **59**, 2592 (1989); G. J. Dolan, G. V. Chandrasekhar, T. R. Dinger, C. Feild, and F. Holtzberg, *ibid.* **62**, 827 (1989); C. A. Bolle *et al.*, *ibid.* **60**, 112 (1991), D. J. Bishop, P. L Gammel, D. A. Huse, and C. A. Murray, Science **255**, 165 (1992).

[6]D. Cribier, B. Jacrot, L. M. Rao, and B. Farnoux, Phys. Lett. **9**, 106 (1964); see also J. Schelten, H. Ullmaier, and W.

Schmatz, Phys. Status Solidi B **48**, 619 (1971); J. Schelten, H. Ullmaier, and G. Lippman, Z. Phys. **253**, 219 (1972); J. Low Temp. Phys. **14**, 213 (1974).

[7]R. P. Huebener, *Magnetic Flux Structures in Superconductors* (Springer-Verlag, Berlin, 1979), Chap. 6.

[8]E. M. Forgan, D. K. McPaul, H. A. Mook, P. A. Timmins, H. Keller, S. Sutton, and J. S. Abell, Nature **343**, 735 (1990); E. M. Forgan, D. K. McPaul, H. A. Mook, S. L. Lee, R. Cubitt, J. S. Abell, F. Gencer, and P. A. Timmins, Proceedings of *M^2S-HTSCIII* [Physica C (to be published)]; E. M. Forgan, Physica B **L69**, 107 (1991).

[9]V. G. Kogan, Phys. Lett. **85A**, 298 (1981).

[10]L. N. Bulaevskii, M. Ledvij, and V. G. Kogan, Phys. Rev. B **45**, 366 (1992).

[11]V. G. Kogan, N. Nakagawa, and S. Thiemann, Phys. Rev. B **42**, 2631 (1990).

[12]L. L. Daemen (unpublished).

[13]T. M. Riseman (private communication).

[14]R. P. Brent, *Algorithms for Minimization without Derivatives* (Prentice-Hall, Englewood Cliffs, NJ, 1973), Chap. 5.

[15]M. Doria, Physica C **178**, 51 (1991).

[16]E. H. Brandt (unpublished).

[17]Vinnikov *et al.*, J. Less-Common Met. **164/165**, 1271 (1990).